

A Tethered Façade Cleaning Robot Based on a Dual Rope Windlass Climbing Mechanism: Design and Experiments

Hobyeong Chae^{ID}, Yecheol Moon, KyungUk Lee^{ID}, SungJun Park, Hwa Soo Kim^{ID}, Member, IEEE,
and TaeWon Seo^{ID}, Senior Member, IEEE

Abstract—Cleaning tasks for vertical structures, such as building façades and walls on construction sites, are dangerous; there is a high risk of fall accidents among workers engaged in such tasks. Hence, research on the automation of wall-cleaning tasks based on robotics technology has been actively conducted in recent years. However, existing wall-cleaning robots have limitations, such as poor mobility performance or the need for additional infrastructure for operation. In this article, we designed a novel rope-driven wall-cleaning robot Edelstro-M2 with two innovative characteristics. First, both vertical and horizontal movements on the wall are possible by implementing a dual rope climbing mechanism and parallel kinematics. Second, except for a rope fixing arrangement, additional infrastructure, such as winch and building management unit systems, is not required for operation. A prototype model was developed, and real-world experiments were conducted to verify the mobility and cleaning performance of the robot. In the experiment, the robot was controlled by manual remote control. We plan to study automatic control of the robot in the future works.

Index Terms—Cleaning automation, climbing robot, façade cleaning robot.

Manuscript received 22 November 2021; revised 26 March 2022; accepted 2 May 2022. Date of publication 18 May 2022; date of current version 16 August 2022. Recommended by Technical Editor M. Grebenstein and Senior Editor X. Chen. This work was supported by the National Research Foundation of Korea Grant funded by the Ministry of Science and ICT under the First-Mover Program for Accelerating Disruptive Technology Development under Grant NRF-2018M3C1B9088331 and Grant NRF-2018M3C1B9088332 and by Bridge Convergence R&D Program under Grant NRF-2021M3C1C3096807 and Grant NRF-2021M3C1C3096808. (Hobyeong Chae and Yecheol Moon contributed equally to this work.) (Corresponding author: TaeWon Seo.)

Hobyeong Chae, Yecheol Moon, KyungUk Lee, SungJun Park, and TaeWon Seo are with the School of Mechanical Engineering, Hanyang University, Seoul 04763, South Korea (e-mail: ppweter21@gmail.com; mycm1302@gmail.com; dlruddhr620@gmail.com; redeye223@naver.com; taewon.seo1@gmail.com).

Hwa Soo Kim is with the Department of Mechanical System Design, Kyonggi University, Suwon 16227, South Korea (e-mail: hskim94@kgu.ac.kr).

This article has supplementary material provided by the authors and color versions of one or more figures available at <https://doi.org/10.1109/TMECH.2022.3172689>.

Digital Object Identifier 10.1109/TMECH.2022.3172689

I. INTRODUCTION

THE application of robotics technology across many industries has solved many safety problems and increased work efficiency. A wall-cleaning robot is an example. In the past and even currently, human workers perform wall-cleaning tasks using ladders or ropes; these tasks are extremely dangerous, subjecting humans to a high risk of falling accidents. In the past three years, 39 workers have lost their lives during wall-cleaning tasks in Korea [1].

Safety issues can be solved by automating wall-cleaning tasks using robots. Therefore, many studies have recently been conducted on wall-cleaning robots, and various commercial and research models have been developed that implement diverse methods for robot locomotion and cleaning processes.

For example, Serbot's [2] GEKKO is a commercial robot that is sold after development. It cleans at a speed of $400 \text{ m}^2/\text{h}$ by attaching it to the wall using a rope. Zhang *et al.*'s [3] Sky Cleaner and Qian *et al.*'s [4] dual suction cups are equipped with a vacuum suction autonomous mobile platform for locomotion. Sky Cleaner robots can clean on either a flat glass wall or a curved glass wall with a modest angle between the glasses. The dual suction cup robot can travel across smooth glass surfaces utilizing gravity and the lifting power of the trolley crane on the roof, clinging to the surfaces using twin vacuum suction cups. Kim *et al.*'s [5] Rope Ride, Manntech's [6] façade cleaning, and Schraft *et al.*'s [7] SFRII can move vertically using winch-controlled wire ropes. The Rope Ride robot rides vertically using winch on the building's wall, avoids obstacles on its own, and cleans with enough contact force. Manntech is servicing the wall cleaning of various atypical structures using a vertical winch. SFRII is used to clean the exterior of windows on a facade with vertical jambs and horizontal bars automatically. Wang *et al.*'s [8] Skyboy is an automated cleaning machine designed for reversed inclining glass facades using a magnetic attachment mechanism. Edelstro-M1 [9] developed in our previous studies and Moon *et al.*'s [10] BFMR can reach any part of a building's façade with the help of a building management system (BMS), such as a gondola or guide rail. Edelstro-M1 is a robot that is attached to a gondola, overcomes obstacles with a tristar wheel, and increases the cleaning area with a compliant manipulator. BFMR is a water circulation cleaning tool system attached to a gondola that increases cleaning efficiency and reduces water

usage. A study to classify various wall-cleaning robots and compare their performances was also conducted [11].

However, the existing wall-cleaning robots have several limitations. The suction cup and magnetic attachment method can only be used on limited surface materials; moreover, robots with these mechanisms have low movement speeds and weight limits. Single-wire winch-type robots cannot move in the horizontal direction without relocation of the wire winch; moreover, they are unstable under external forces that act like a pendulum. BMU-integrated robots cannot be used on buildings that have no BMU systems.

In this article, we designed and developed a novel wall-cleaning robot Edelstro-M2 that combines the advantages of existing models. The two main contributions of our study are as follows.

- 1) First, the parallel rope control using the dual rope climbing mechanism allows high mobility with free movement in both the horizontal and vertical directions on the wall. In addition, owing to the dual rope configuration, the resistance to external forces is much higher than that of the single wire type.
- 2) Second, installation of additional infrastructures, such as electric wire winches or a BMU system, is unnecessary; the robot can be used on any type of wall by simply fixing a pair of ropes.

The rest of this article is organized as follows. In Section II, the locomotion strategies of the robot are described. Section III introduces the mechanical modules of the robot and their theoretical backgrounds. Section IV introduces details of the prototype model of Edelstro-M2. In Section V, the experimental setup and scenarios are introduced, including an analysis of the experimental results. Finally, Section VI concludes this article.

II. LOCOMOTION STRATEGIES

A. Two-DOF Locomotion

The main innovative characteristic of Edelstro-M2 is the capability of omnidirectional locomotion on vertical wall. While most robots developed can move only in the vertical direction, the proposed model can move freely on the wall (2-DOF). In addition, the locomotion of the robot can be generated by the robot itself, rather than an external power source, such as an electric wire winch fixed to the roof of the buildings or on the ground. A comparison between the conventional and the proposed parallel rope-driven methods for the locomotion of a wire-driven-type wall-cleaning robot is shown in Fig. 1.

B. Kinematic Analysis

Parallel kinematics were designed to implement the 2-DOF motion of the robot. Fig. 2 shows the robot hanging on the ropes, indicating its position, length, and angle of the rope, where A_1 and A_2 are end points of the rope, O_R is origin point of the robot, l_1 and l_2 are the lengths of the left and right ropes, θ_1 and θ_2 are the angles between the vertical line and the ropes, and W is the distance between the fixing points of the rope on the wall.

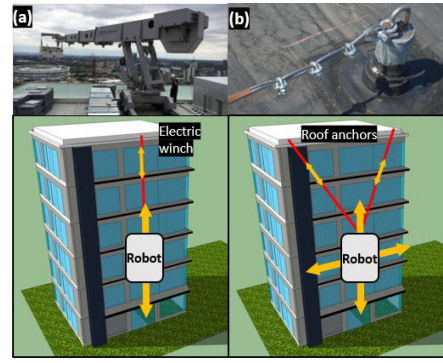


Fig. 1. Comparison between conventional and proposed locomotion strategies. (a) Electric winch needs to be placed on the rooftop or on the ground. The robot can only move along a vertical path. (b) Only two rope fixings are required. The robot can achieve 2-DOF motion on the wall.

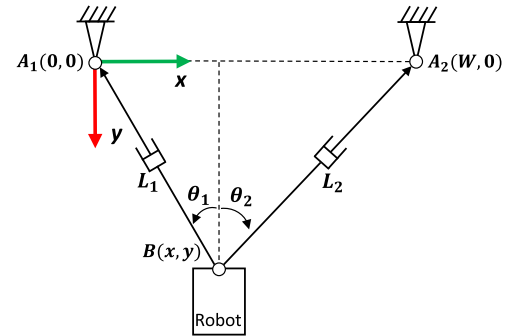


Fig. 2. Kinematic diagram of the proposed robot. The robot is connected parallel to the wall by a pair of ropes. The main goal of kinematic analysis is to find forward kinematics and the Jacobian matrix from the constraint equations of each variable.

For localization of the robot, forward kinematics are used to calculate the position of the robot because there are no global localization methods implemented. θ_1 and θ_2 are more stable than l_1 and l_2 . This is because when a rope slip occurs, the error of the rope length accumulates. Consequently, the position of the robot (x, y) is derived as follows:

$$[x \ y]^T = W \left[\frac{\tan \theta_1}{\tan \theta_1 + \tan \theta_2} \ \frac{1}{\tan \theta_1 + \tan \theta_2} \right]^T. \quad (1)$$

For locomotion of the robot, the climbing mechanisms adjust the length of each rope (l_1, l_2). To control the velocity of the robot in the Cartesian coordinate system (\dot{x}, \dot{y}) by controlling the rope length, it is necessary to obtain a Jacobian matrix by differentiating the constraint equations. The Jacobian matrix is a function of the rope angles (θ_1, θ_2). The relation between velocity, rope length, and angle is defined in the following equation:

$$[\dot{l}_1 \ \dot{l}_2]^T = J [\dot{x} \ \dot{y}]^T \quad (2)$$

where \dot{l}_1 and \dot{l}_2 are the differentiation of each rope length, J is the Jacobian matrix, and \dot{x} and \dot{y} are the velocities of the robot in the Cartesian coordinate system. A more specific form of the

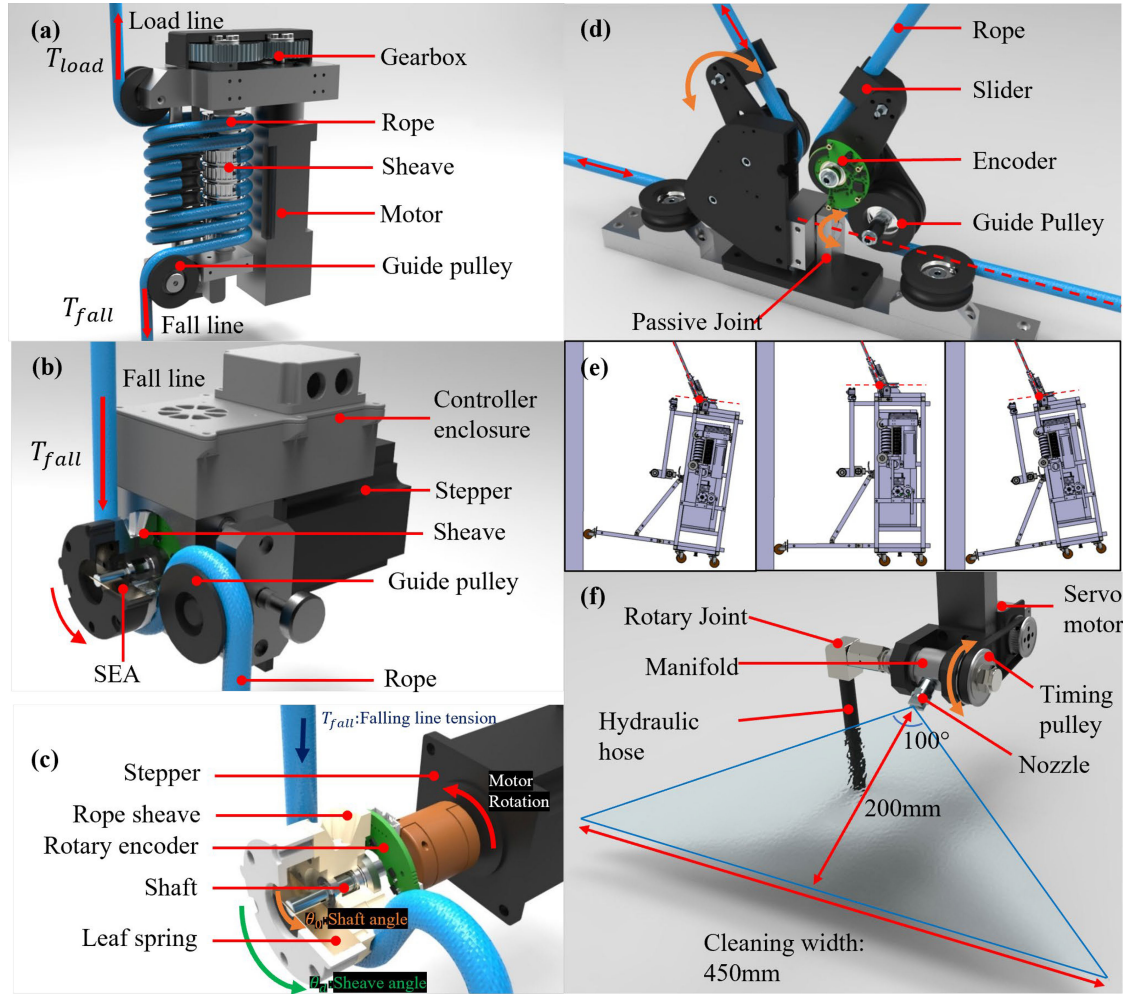


Fig. 3. Structure of each part of the robot. (a) Windlass-type rope-climbing module. (b) Tensioner module. (c) Structure of the SEA mechanism. (d) Rope-angle-sensing module. (e) Owing to the design wherein the rotation angles of the passive joint and exiting rope are the same, the module can cope with roll orientation change of the robot, minimizing changes in the rope lengths. (f) High-pressure cleaning module.

Jacobian matrix is given by the following equations:

$$J = J_2 \ J_1^{-1} \quad (3)$$

$$J_1 = W \begin{bmatrix} \frac{\sec^2 \theta_1 \tan \theta_2}{(\tan \theta_1 + \tan \theta_2)^2} & \frac{-\sec^2 \theta_2 \tan \theta_1}{(\tan \theta_1 + \tan \theta_2)^2} \\ \frac{-\sec^2 \theta_1}{(\tan \theta_1 + \tan \theta_2)^2} & \frac{-\sec^2 \theta_2}{(\tan \theta_1 + \tan \theta_2)^2} \end{bmatrix} \quad (4)$$

$$J_2 = W \begin{bmatrix} \frac{-\cos \theta_2 \cos(\theta_1 + \theta_2)}{\sin^2(\theta_1 + \theta_2)} & \frac{-\cos \theta_2 \cos(\theta_1 + \theta_2) - \sin \theta_2 \sin(\theta_1 + \theta_2)}{\sin^2(\theta_1 + \theta_2)} \\ \frac{-\cos \theta_1 \cos(\theta_1 + \theta_2) - \sin \theta_1 \sin(\theta_1 + \theta_2)}{\sin^2(\theta_1 + \theta_2)} & \frac{-\cos \theta_1 \cos(\theta_1 + \theta_2)}{\sin^2(\theta_1 + \theta_2)} \end{bmatrix}. \quad (5)$$

III. MODULAR CONFIGURATION

A. Rope Selection

Rope is divided into two types rope: static rope and dynamic rope. Static ropes have higher stiffness than dynamic ropes. High rope stiffness means less change in rope length, which is advantageous for accurate control. The ascender lifting this robot causes kinetic friction. In order to prevent abrasion, the skin of the rope must have high strength. The type of rope varies depending on the company, but the one that meets this requirement is the Kemmantel type. Kemmantel type is a type

of rope that has a sheath in the core, and is mainly used by many commercial friction ascenders. Among these Kemmantel-type ropes, we chose Edelied Super Static Linktech 11-m rope, which is the strongest and has less separation between the skin and the core of the rope. The tensile strength of this rope is 3.3 kN, which is sufficient for the robot's weight of 60 kg. The static elongation is 3.7%, which is suitable for control because there is little deformation.

B. Rope Climbing Module

The rope climbing capability was implemented using a windlass-type climbing module with the Capstan mechanism. Fig. 3 describes the structure of the climbing module and the forces acting on it.

The rope can be pulled or released by rotating the multistage rope sheave using a servo motor. The following Capstan equation shows the relationship between the tensile force and the frictional force at both ends of the rope wound around the sheave to prevent rope slip [12]:

$$T_{fall} = \frac{T_{load}}{e^{\mu_k \theta}} \quad (6)$$

TABLE I
MECHANICAL CHARACTERISTICS OF THE ROPE CLIMBING MODULE

Symbol	Value	Unit	Remark
T_{load}	513*	N	Total mass: 60 kg Max rope angle: 30° Max acceleration: 1.5 m/s ²
μ_k	0.14	-	Experimental data
θ	25.1	rad	Eight times wound with half contact angle
T_{fall}	35.3	N	Required fall line tension

Note: *Calculated from rope kinematics.

where T_{fall} and T_{load} are the tensions on the fall and load lines, respectively, μ_k is the kinetic friction coefficient between the rope and sheave, and θ is the total wound angle of the rope.

The equation must be satisfied to prevent rope slip. Based on the design variables of the experimental data, the minimum fall line tension was determined. The variables are listed in Table I.

It is necessary to maintain the fall line tension of the climbing module above a certain level to prevent rope slippage on the rope sheaves. The simplest method is to hang a weight at the rope end. However, this method increases the weight of the robot and risk of accidents.

Therefore, we devised a tensioner module that maintains the fall line tension of the climbing module at a specific level. The tensioner consists of a grooved rope sheave and stepper that can grasp and pull the fall line rope. A rotary serial elastic actuator (SEA) mechanism [13] was adopted for torque control. The overall configuration of the tensioner module is shown in Fig. 3(b) and (c).

The core element of the tensioner's SEA mechanism is the leaf spring, which is an elastic element that connects the motor shaft and sheave. When the motor shaft rotates, the leaf spring deforms while generating torque to the sheave. Eventually, the torque is transferred to the rope and acts as a fall line tension. The leaf spring can be mechanically modeled as a fixed-end beam, which shows a linear relationship between the deformed angle and moment applied to the center point when deformation does not occur, yielding of the spring. The desired deformation angle θ_d to generate the desired moment M can be derived as follows:

$$\theta_d = \frac{ML}{16EI} \quad (7)$$

where E is the elastic modulus of the spring, I is the moment of inertia of the spring's longitudinal section, and L is the length between the spring fixing points. A detailed view of the leaf spring mechanism and the relationship between the deformed angle and moment obtained from the experiment are shown in Fig. 4.

C. Rope-Angle-Sensing Module

As mentioned previously, it is necessary to measure the angle of the rope connected to the robot for kinematic analysis. The rope-angle-sensing module has two roles to play. First, it measures the rope angle data accurately with a sensing frequency

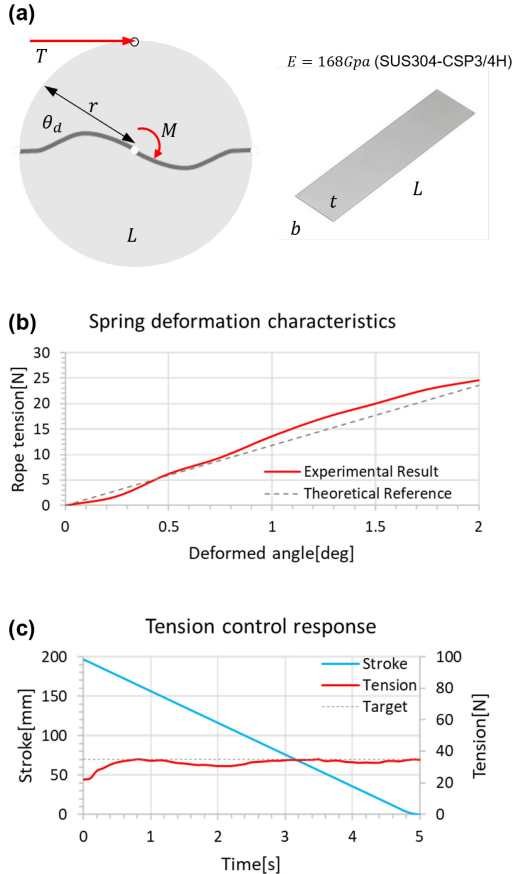


Fig. 4. (a) Mechanical model (fixed-end beam) and geometry of the spring. (b) Spring deformation characteristics obtained from a test. The actual spring stiffness is 704 N/rad and theoretical value is 676 N/rad. (c) Result of dynamic response from the active tensioner. The rope is pulled with constant speed and a simple proportional derivative controller maintains the target tension, which verified feasibility of the tensioner module.

higher than that of the control loop of the robot. Second, it can accept the movement of ropes and the change in the robot's orientation such that they do not affect the sensor measurement value. To accomplish these requirements, the rope-angle-sensing module is equipped with a high-resolution absolute rotary encoder and rope guiding mechanism.

The rope-angle-sensing module has a passive point to cope with changes in the roll orientation of the robot. If a change in the rope length occurs, the control performance may be adversely affected. As a result, to minimize the change in rope length due to joint rotation, the axis through which the rope exits coincides with the joint rotation axis. The overall configuration and joint rotation examples are presented in Fig. 3(d) and (e).

D. High-Pressure Cleaning Module

For simplicity and versatility, a high-pressure spraying nozzle was used as the cleaning device. High-pressure cleaning has several advantages. First, despite the nonuniformity of the target surface, this method shows robust cleaning performance compared to other methods, such as brushing and mopping, which have unclean portions in uncontacted areas. Second, it is advantageous for weight reduction in small-sized wall-cleaning robots

TABLE II
MECHANICAL SPECIFICATIONS OF THE PROTOTYPE MODEL

Parameter	Value
Dimensions	W820 mm×H1000 mm×D600 mm
Weight (w/ and wo/ enclosure parts)	60 kg / 48 kg
Maximum workspace height	20 m (in experiment)
Climbing module load capacity	90 kg for single module
Tensioner module load capacity	36 N for single module
Rope-angle-sensing resolution	0.0027°
Maximum nozzle pressure	190 bar
Rope specification	11 mm dia. kernmantle rope

[14]. The components of the high-pressure cleaning module are small and lightweight elements, such as nozzles, manifolds, and hoses. Conversely, other methods, such as powered brushes, require heavy electric motors, transmission mechanisms, and cleaning brush parts. Therefore, high-pressure cleaning is the most suitable cleaning method for the proposed robot because the robot has to deal with irregular surface structures during the cleaning process, and safety issues will occur with excessive weight.

The module consists of a nozzle, manifold, and rotation mechanism. The nozzle is made of tungsten carbide, which exhibits high wear resistance under a high-pressure environment. The manifold connects the nozzle and rotation mechanism, providing a rotary joint for the flowing path. The rotation mechanism can control the spraying direction of the nozzle using a small position controllable waterproof servo motor, which improves the flexibility of the cleaning process. An external pump with a valve that controls the flow rate and pressure provides high-pressure water. The overall configuration of the high-pressure cleaning module is shown in Fig. 3(f).

IV. PROTOTYPE MODEL

A. Mechanical System

A prototype model was developed to verify the robot's operation and cleaning performance through field experiments. The mechanical system of the robot includes a climbing and tensioner module, rope-angle-sensing module, and cleaning module described in Section III. Each module was integrated into the main frame of the robot. The overall configuration of the mechanical system and the details of each module are shown in Fig. 5. The specifications of the performance of each module included in the mechanical system are summarized in Table II.

B. Electronic System

An electronic system has been designed to perform power distribution, interface, main control loop operation, etc. Electronic components are inside the enclosure box to protect the components from external moisture and dust. The electronic system of the robot requires an ac power source and Ethernet connection. The robot also has a backup wireless radio

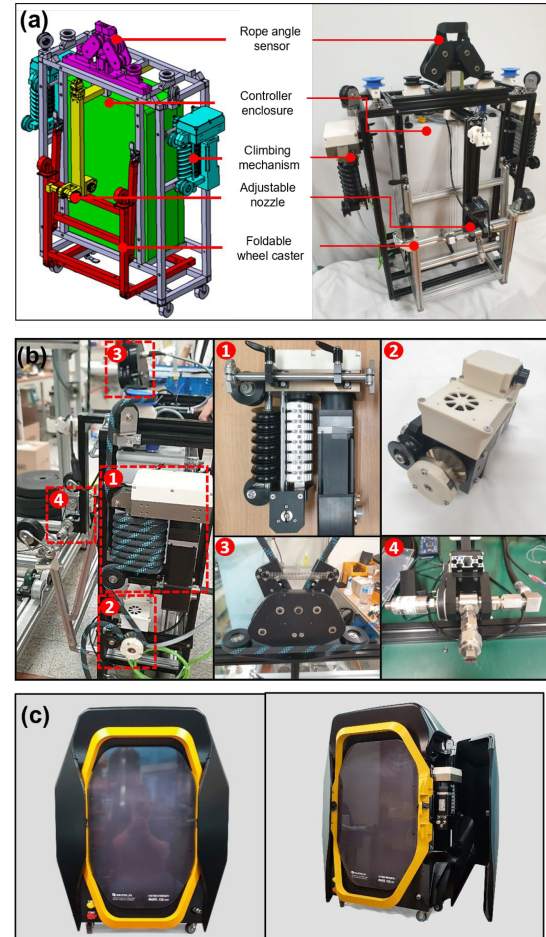


Fig. 5. Configuration of the prototype model. (a) CAD modeling and image of the prototype model describing mechanical modules of the robot. (b) Prototypes of every module explained in Section III. (1) Rope climbing module. (2) Tensioner module. (3) Rope-angle-sensing module. (4) High-pressure cleaning module. (c) Commercial concept model. Mock-up parts of external enclosure were assembled to form the prototype.

control interface when the connection is broken. The electronic system of the prototype model is shown in Fig. 6 and Table III.

V. EXPERIMENTAL RESULTS

A. Experimental Setup

As mentioned previously, the main purpose of developing a prototype model is to conduct field experiments on a real-world building wall. The experiments were conducted on a concrete wall with a width of 8 and 10 m height. A pair of ropes was fixed to the rooftop, and the robot was attached to the rope. The user controls the robot on the ground using radio control equipment and a monitoring system. It is manual control by user, not automatic control. The external pump was located on the ground to provide water for the high-pressure cleaning module of the robot.

One of the most important aspects of the experimental setup is the contamination condition of the wall. As repeatability is

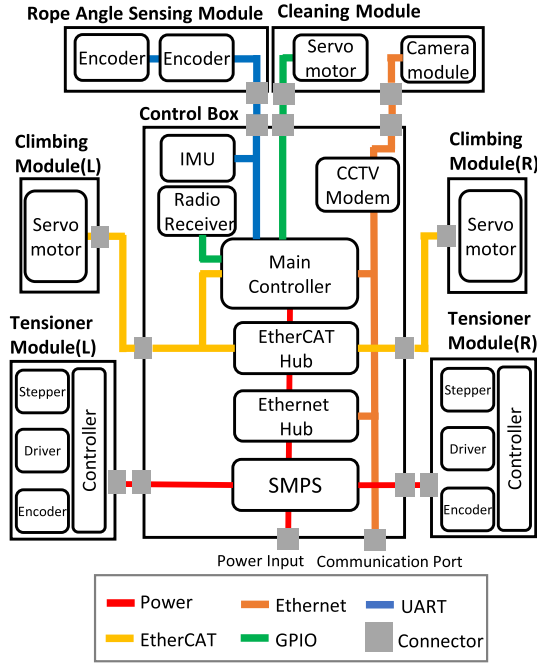


Fig. 6. Wiring diagram of the robot's electronic system. External ac power needs to be supplied through the input connector at the bottom. SMPS generates dc voltage and distributes power to every electronic component. The Ethernet is connected to the main controller, CCTV, and remote user PC; this configuration makes it possible to remotely control the robot and perform the cleaning task. The servo motors of the climbing module are controlled via EtherCAT protocol, which shows fast response and synchronization performance [15].

TABLE III
ELECTRONIC SYSTEM PART LIST

Module	Component	Manufacturer	Model
Control box	SMPS	Mean Well	HRPG-1000-48
	Main controller	NI	cRIO-9042
	GPIO interface	NI	NI 9401
	EtherCAT hub	Omron	GX-JC06
	IMU	E2BOX	EBIMU-9DOFv5
	CCTV modem	Hanwha Techwin	XNB-6001
	Radio receiver	Spektrum	AR610
Climbing module	Servo motor	Maxon	IDX56L
Tensioner module	Controller	PJRC	Teensy4.0
	Stepper driver	Trinamic	TMC5160
	Stepper motor	Stepper express	23HS8425
	Encoder	RLS	Orbis
Rope-angle-sensing module	Encoder	RLS	AksIM-2
Cleaning module	Servo motor	CiLAB	D30
	Camera lens	Hanwha Techwin	SLA-T4680

important for accurate evaluation, artificial contamination using color pigments was used instead of natural contamination. The overall experimental setup is shown in Fig. 7.

B. Mobility Performance

One of the main contributions of Edelstro-M2 is its high mobility performance. It can move faster than other wall-cleaning robots and has the ability of omnidirectional locomotion.

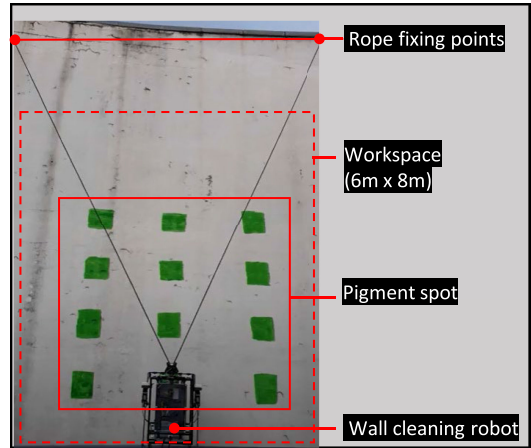


Fig. 7. Experimental setup where prototype of the wall-cleaning robot was allowed to hang on a pair of fixed ropes and green colored pigment spots were arranged in grid shape to implement artificial contamination of the wall.

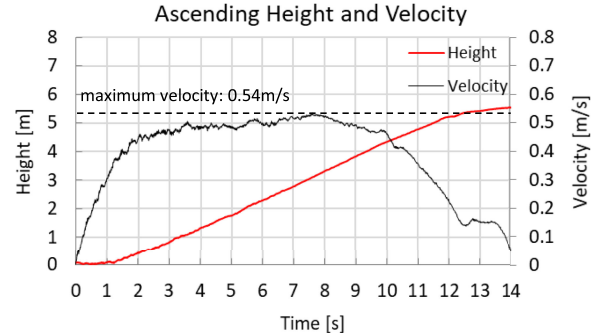


Fig. 8. Robot's position and velocity data while ascending. Total ascended height was 5.5 m and trapezoidal motion profile was applied. The maximum speed was about 0.54 m/s.

The first experimental scenario was to measure the vertical movement speed of the robot. During the experiment, the robot ascended approximately 6 m in the vertical direction while the position and speed of the robot were recorded using an IMU and kinematic calculation by using encoder. The results of the first experimental scenario are presented in Fig. 8.

The robot moved 5.5 m at a maximum speed of 0.54 m/s for 14 s. During the movement, the height does not change compared to the speed change during the first 1 s. It is because the rope is not completely in contact with encoder. When setting up the robot for the first time, the rope is loosened to adjust the starting position. Because of it, the encoder does not rotate because the rope does not contact the encoder properly. So, the robot moves 5.5 m instead of 6 m, and an error of 8% occurred.

In the case of a sharp decrease starting from 9.7 s, it occurred because of the step difference in the cement wall in the middle. The robot was slightly caught in this step. It is thought that the error occurred because of this jamming.

In addition, based on the data from the first experimental scenario, a performance comparison with existing robot models was conducted. As summarized in Table IV, the Edelstro-M2 showed superior wall-climbing performance compared to commercial

TABLE IV
CLIMBING SPEED COMPARISON OF WALL-CLEANING ROBOTS

Model	Locomotion	Absolute speed [m/s]	Body length /s
Gekko façade [2]	Suction	0.13	0.107
Sky cleaner [3]	Suction	0.035	0.245
Dual suction cup [4]	Suction	0.035	0.02
Rope ride [5]	Rope/Wire	0.26	0.175
Façade cleaning [6]	Rope/Wire	0.055	0.015
SFRII [7]	Rope/Wire	0.02	0.02
Skyboy [8]	Rope/Wire	0.19	0.14
Edelstro-M1 [9]	BMU assisted	0.12	0.3
BFMR [10]	BMU assisted	0.07	0.044
Edelstro-M2	Rope/Wire	0.54	0.45

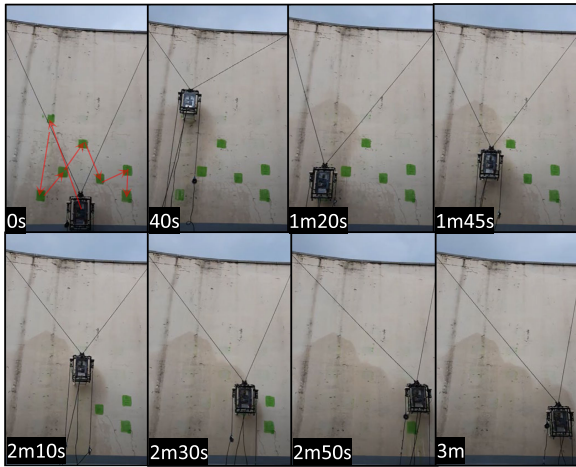


Fig. 9. Entire process of the second experimental scenario. It took 3 min to clean seven contamination spots sequentially and return to the starting position. No manipulation was needed except the remote control of the robot (video is available in the multimedia extension).

and research models in terms of both absolute speed and relative speed based on body length.

The second experimental scenario was to verify the robot's omnidirectional movement performance, which means that the robot should be able to reach any specific target position in the workspace. Owing to this omnidirectional locomotion capability, it is possible to reduce the working time of the robot and increase the cleaning efficiency compared to the existing single-wire-type robot, where a user must relocate the robot to change its horizontal position on the wall.

For verification, pigment spots were randomly placed around the workspace. The robot approached them sequentially and washed off the spots. During this operation, the user did not manipulate any process except for the remote control. Even at the boundary of the workspace, the cleaning performance remains constant. This is because the workspace is set smaller than the actual movable area, and the position and the performance of the nozzle do not matter.

Fig. 9 shows the entire process of the second experimental scenario; the elapsed time stamps are marked on the images.

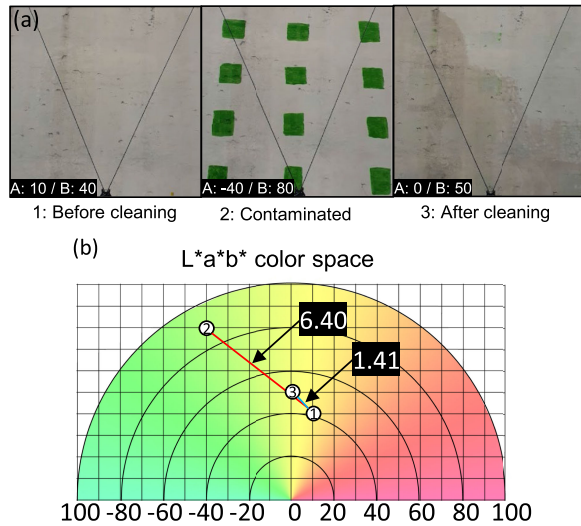


Fig. 10. (a) Images of three different cleaning conditions. (1) Initial condition before cleaning. (2) Contaminated condition with green pigment spots arranged in grid shape. (3) Cleaned condition after a cycle of high-pressure cleaning process. (b) Coordinates of each condition on $L^*a^*b^*$ color space. The distance between the coordinates corresponds to color difference, which can be analyzed as the contamination level of the target surface.

C. Cleaning Performance

It is not easy to measure the cleaning performance because different standards may be applied depending on the material of the target surface and the types of contamination. In our experimental setup, a brightly colored concrete surface, where no patterns or textures exist, was selected as the target. Bright color and pattern wall has the advantage of high visibility when it is stained a specific color. To quantify the contamination state of the wall, it is necessary to analyze the proportion of the color where contamination exists. Cleaning performance can be quantified by comparing the color analysis results for three conditions: initial, contaminated, and cleaned.

We adopted the $L^*a^*b^*$ color space model to analyze color. The $L^*a^*b^*$ space is a color space calibrated for human color perception. It means that the Euclidean distance between two different colors in the color space coordinate system corresponds approximately to the color difference perceived by the human eye [16]. Owing to these advantages, $L^*a^*b^*$ color space has been applied in various research for color change analysis in the dental [17], dermatology [18], agricultural [19], and civil engineering [20] fields.

The third experimental scenario is to numerically obtain the cleaning performance by analyzing the $L^*a^*b^*$ color difference between the three different cleaning conditions. The a^* value represents the intensities of yellow (high) and blue (low), and the b^* value represents the intensities of red (high) and green (low). The L^* value represents luminosity, which is not affected by the color changes. The color of the pigment was determined to be green to maximize the color change effect by artificial contamination. The spots were placed in the shape of a grid in a specific area where the images were taken. The details and results of the third experimental scenario are described in Fig. 10.

According to the results, the color difference between conditions 1 and 3 was 1.41, and conditions 2 and 3 was 6.4, which means that the color difference of the fully contaminated condition was 7.81. Thus, it can be concluded that about 82% of the contamination was removed after a cycle of cleaning process.

D. Limitation of Performance

The limitations of the robot's performance are caused by the unwanted movement and nozzle.

Rotation of the robot occurred because the distance between the left and right of the rope-angle-sensing module was short. Due to the step difference between the two contact points between the robot and the facade, the robot rotates in the yaw direction. Therefore, the nozzle also rotates, and it makes limit to the cleaning area. In addition, if the wall is rough surface, vibration is generated because the step is continuously repeated. These vibrations reduce the durability of the robot and make it difficult to control.

Another limitation of the robot is the limitation of the nozzle. The cleaning performance of the robot is determined by the water pressure of the nozzle. If there is a place in the cleaning area that does not reach water, cleaning is impossible. In addition, if the step difference between the two contact points increases, the distance between the nozzle and the wall increases. As the distance between the nozzle and the wall increases, the water pressure decreases. It means the cleaning performance decreases.

VI. CONCLUSION

In this article, we proposed a wall-cleaning robot Edelstro-M2 that combines the advantages of existing models. Existing models require additional infrastructure or frequent relocation to operate. Edelstro-M2 has two distinguishing features. First, the parallel control of the dual rope climbing mechanism allows free movement in both the horizontal and vertical directions on the wall. Second, installation of additional infrastructures, such as electric wire winch or BMU system, is unnecessary; it can be used on any type of wall by simply fixing a pair of ropes.

To implement the omnidirectional movement of the proposed robot, a dual rope climbing mechanism was devised; a kinematic analysis was conducted for both position estimation and velocity control. Edelstro-M2 has a modular design and is composed of five modules.

A prototype model was developed, and field experiments were conducted on the real-life building. Several experimental scenarios were established to evaluate the mobility and cleaning performance of the robot. The results showed that the robot can reach absolute speed of 0.52 m/s and the omnidirectional movement capability was verified. The cleaning performance of the robot was evaluated using the $L^*a^*b^*$ color space analysis. The results showed that approximately 82% of the contamination was removed.

In future research, we will implement the global localization capability of the robot for fully automated motion control and

path planning. Instead of manual control, automatic control will be applied so that the cleaning is automatically carried out when the location of the contaminants is specified. In addition, real-time contamination detection should be applied to the high-level automation of the cleaning process. The ultimate goal is to create a robot that detects contamination and performs cleaning on the real time.

REFERENCES

- [1] The Hankyoreh, 2021. Accessed: Nov. 15, 2021. [Online]. Available: <https://www.hani.co.kr/arti/society/labor/1013761.html>
- [2] SERBOT. GEKKO Façade Robot, 2021. Accessed: Nov. 15, 2021. [Online]. Available: <https://www.serbot.ch/en/facades-surfaces-cleaning/gekko-facade-robot>
- [3] H. Zhang, J. Zhang, W. Wang, R. Liu, and G. Zong, "A series of pneumatic glass-wall cleaning robots for high-rise buildings," *Ind. Robot.: Int. J.*, vol. 34, no. 2, pp. 150–160, 2007.
- [4] Z. Qian, Y. Zhao, Z. Fu, and Q. Cao, "Design and realization of a non-actuated glass-curtain wall-cleaning robot prototype with dual suction cups," *Int. J. Adv. Manuf. Technol.*, vol. 30, pp. 147–155, 2006.
- [5] T. Kim *et al.*, "Design and control of a cleaning unit for a novel wall-climbing robot," *Appl. Mechanics Mater.*, vol. 541, pp. 1092–1096, 2014.
- [6] Manntech. Façade cleaning systems, 2021. Accessed: Nov. 15, 2021. [Online]. Available: <https://www.manntech.com/solutions/>
- [7] R. D. Schraft, U. Brauning, T. Orlowski, and M. Hornemann, "Automated cleaning of windows on standard facades," *Automat. Construction*, vol. 9, pp. 489–501, 2000.
- [8] W. Wang, B. Tang, H. Zhang, and G. Zong, "Robotic cleaning system for glass facade of high-rise airport control tower," *Ind. Robot.: Int. J.*, vol. 37, no. 5, pp. 469–478, 2010.
- [9] H. Chae *et al.*, "Façade cleaning robot with manipulating and sensing devices equipped on a gondola," *IEEE/ASME Trans. Mechatronics*, vol. 26, no. 4, pp. 1719–1727, Aug. 2021.
- [10] S. M. Moon, C. Y. Shin, J. Huh, K. W. Oh, and D. Hong, "Window cleaning system with water circulation for building façade maintenance robot and its efficiency analysis," *Int. J. Precis. Eng. Manuf.-Green Technol.*, vol. 2, no. 1, pp. 65–72, Jan. 2015.
- [11] T. Seo, Y. Jeon, C. Park, and J. Kim, "Survey on glass and façade-cleaning robots: Climbing mechanisms, cleaning methods, and applications," *Int. J. Precis. Eng. Manuf.-Green Technol.*, vol. 6, no. 2, pp. 367–376, Mar. 2019.
- [12] K. L. Johnson, *Contact Mechanics*. New York, NY, USA: Cambridge Univ. Press, 1985.
- [13] Y. Kim, J. Lee, and J. Park, "Compliant joint actuator with dual spiral springs," *IEEE/ASME Trans. Mechatronics*, vol. 18, no. 6, pp. 1839–1844, Dec. 2013.
- [14] D. Yoon, S. Ryu, J. Hong, Y. Lee, and T. Seo, "Empirical optimization and evaluation for multi-nozzle cleaning device," *Int. J. Precis. Eng. Manuf.*, vol. 22, no. 7, pp. 1229–1236, May 2021.
- [15] R. Delgado, S.-Y. Kim, B.-J. You, and B.-W. Choi, "An EtherCAT-based real-time motion control system in mobile robot application," in *Proc. 13th IEEE Int. Conf. Ubiquitous Robots Ambient Intell.*, 2016, pp. 710–715.
- [16] K. León, D. Mery, F. Pedreschi, and J. León, "Color measurement in $L^*a^*b^*$ units from RGB digital images," *Food Res. Int.*, vol. 39, no. 10, pp. 1084–1091, Dec. 2006.
- [17] R. R. Seghi, E. R. Hewlett, and J. Kim, "Visual and instrumental colorimetric assessments of small color differences on translucent dental porcelain," *J. Dent. Res.*, vol. 68, no. 12, pp. 1760–1764, Dec. 1989.
- [18] I. L. Weatherall and B. D. Coombs, "Skin color measurements in terms of CIELAB color space values," *J. Invest. Dermatol.*, vol. 99, no. 4, pp. 468–473, Oct. 1992.
- [19] M. García-Marino, M. L. Escudero-Gilete, F. J. Heredia, M. T. Escriban-Bailón, and J. C. Rivas-Gonzalo, "Color-copigmentation study by tristimulus colorimetry (CIELAB) in red wines obtained from Tempranillo and Graciano varieties," *Food Res. Int.*, vol. 51, no. 1, pp. 123–131, Apr. 2013.
- [20] G. Lemaire, G. Escadeillas, and E. Ringot, "Evaluating concrete surfaces using an image analysis process," *Construction Building Mater.*, vol. 19, no. 8, pp. 604–611, Oct. 2005.